ELSEVIER

Sensors and Actuators B 38–39 (1997) 122–129

SENSORS AND ACTUATORS B CHEMICAL

A microoptode array for fine-scale measurement of oxygen distribution

Gerhard Holst *, Ronnie N. Glud, Michael Kühl, Ingo Klimant [1]

Max-Planck-Institute for Marine Microbiology, Microsensor Research Group, Celsiusstraße 1, D-28359 Bremen, Germany

Abstract

A new microoptode array is presented that provides simultaneous measurement with eight oxygen microoptodes using a simple optical setup and a phase-angle detection principle. The measuring system consists of: (1) an optical unit with eight oxygen microoptodes, a special fiber-coupler array, optical filters, lenses, light sources (light-emitting diodes) and light detectors (photodiodes, photomultiplier tube); (2) a signal-processing unit with analog signal processing (phase-angle detection, filtering) and digital signal processing (control, data storage and display). The oxygen concentration is measured with tapered silica-glass fibers (tip diameter 20–30 μm) by the dynamic quenching of a luminophore. A phase-modulation technique is used to determine the phase-angle shift that is caused by the fluorescence lifetime when the indicator is excited sinusoidally. In a time multiplex mode each sensor signal is sampled. This multisensor array system is designed for the investigation of the oxygen distribution in biofilms and aquatic sediments. The new measuring system and first applications in artificial and natural systems are presented.

Keywords: Microoptodes; Oxygen microsensors; Phase modulation; Fluorescence lifetime sensing; Oxygen optodes; Fluorescence quenching

1. Introduction

The spatial distribution of chemical and physical parameters, e.g., analyte concentrations or temperature, in most natural environments is heterogeneous [1]. By use of microsensors, point measurements and the one-dimensional distribution of chemical parameters, e.g., oxygen, can be resolved at a high spatial resolution. However, to assess the horizontal heterogeneity many point measurements are necessary. Furthermore, the dynamic change of, e.g., oxygen concentration at different points requires simultaneous fine-scale measurements.

So far most data are obtained with microelectrodes [2], but as it is a time consuming and complex procedure to make them, we have initiated the development and application of optical microsensors [3,4] and optoelectronic measuring systems [5]. In the present study a higher integration of measuring channels into a microoptode array was realized to reduce the instrumental efforts that are necessary for parallel measurements. The optical and optoelectronic components of the microoptode system are presented as well as some examples of applications in aquatic environments.

* Corresponding author. Phone: +49 421 2028 834. Fax: +49 421 2028 690. E-mail: gerhardh@postgate.mpi-mm.uni-bremen.de.

[1] Present address: Institut für Analytische Chemie, Bio- und Chemosensorik, Universität Regensburg, D-93040 Regensburg, Germany.

PII S0925-4005(97)00038-5

2. Oxygen microoptode

2.1. Sensor chemistry and calibration

As the basic oxygen-sensing mechanism, the well-known dynamic or collisional quenching of luminescence was applied [3–6,8–12,17,18]. The presented results were obtained with two types of indicators that are described in Table 1. Sensor A consists of ruthenium-II-tris-4,7,diphenyl-1,10-phenanthroline-ClO_4 [3,12,13,17] immobilized in a polystyrene matrix that showed a good mechanical stability, which is necessary for penetration of media like quartz sand. The indicator can be excited with the light of a blue light-emitting diode (LED) and the emission can be detected by photodiodes or, in our case (because of the small signals), by photomultiplier tubes (PMT). The evaluation of the luminescence signal is based on a phase-modulation technique (see Section 3.1. for details), so the modulation frequencies used are given in Table 1. For sensor A the frequency was $f_{mod} = 44.7$ kHz [5]. Sensor B consists of platinum-octaethylporphine, also immobilized in polystyrene [11,18]. This indicator showed longer lifetimes and higher quenching constants, i.e., a larger signal change (see Table 2), but a poorer photostability than indicator A. Indicator B can also be excited by a blue or a blue–green LED and detected by a PMT, but with a lower modulation frequency of $f_{mod} = 5.3$ kHz.

Table 1
Oxygen indicators

Type	Indicator	Matrix	$\lambda_{ex}/\lambda_{em}$ [nm]	f_{mod} [kHz]
Sensor A	ruthenium-II-tris-4,7,diphenyl-1,10-phenanthroline-ClO_4	polystyrene	450/600	44.7
Sensor B	platinum-octyethyl-porphine	polystyrene	400, 530/645	5.3

Table 2
Measuring system performance for both sensor types

Sensor	Oxygen in H_2O [% air saturat.]	Phase angle [°]	Resolution [±°]	Accuracy [±°]	Accuracy [% air saturat.]
Type A	0	50.42	±0.035	±0.07	±0.98
Type A	100	44.21	±0.035	±0.07	±1.3
Type B	0	70.19	±0.035	±0.09	±0.12
Type B	100	33.61	±0.035	±0.09	±0.35

The sensors were calibrated by a two-point calibration [3]. For most of the applications in marine sediments these two points are inherent to the measurement itself. The starting point in the overlying water phase is usually air saturated and while penetrating into the sediment one always reaches zero oxygen in the deeper layers. So both points are measured and give the calibration points. To convert the measured data, two different equations were applied according to the type of sensor. Earlier experiments [3] have shown that for sensor A a modified Stern–Volmer equation was best fitted to the calibration data:

$$\frac{\tau}{\tau_0}=\frac{0.85}{(1+K_{SV}[O_2])}+0.15 \quad (1)$$

(τ=luminescence lifetime, τ_0=luminescence lifetime at zero oxygen, K_{SV}=quenching constant, $[O_2]$=oxygen concentration).

For sensor B, however, an ideal Stern–Volmer [7] equation was used:

$$\frac{\tau}{\tau_0}=\frac{1}{(1+K_{SV}[O_2])} \quad (2)$$

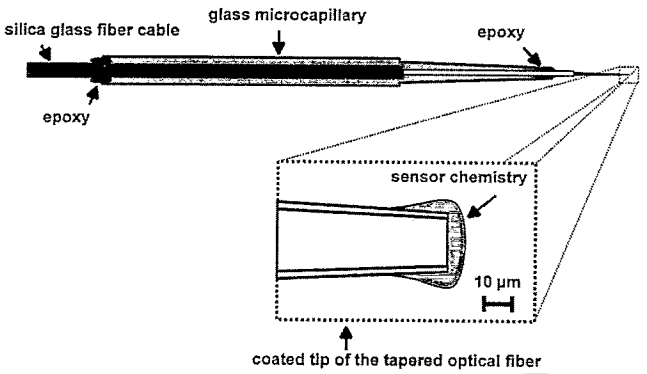

Fig. 1. Schematic drawing of an oxygen microoptode: the tapered silica-glass fiber is fixed with epoxy in a glass microcapillary for better handling. The oxygen indicator layer (see insert) is applied by dip-coating.

For the calibration with the luminescence lifetimes the average or apparent lifetime was used.

2.2. Microoptode

The optical oxygen microsensor basically consisted of a 100/140 µm step-index silica glass fiber cable that was supplied with a standard ST-glass fiber plug at one end. The fabrication procedure was as follows:

1. The PVC tube and the protective coating at the free end of the fiber were removed over a length of approximately 40 mm
2. The bare fiber was tapered in a hot flame to a tip diameter ≈5–10 µm
3. The taper was cut to a tip diameter between 10 and 30 µm (usually a compromise between signal size and small diameter)
4. The taper was dip-coated with an indicator solution. This process was controlled in such a way that the sensor was dipped not more than 20 µm into the 'sensor cocktail'
5. The solvent had to evaporate for about 24 h before the sensor was ready to use. Additionally the microoptode might be coated with carbon black silicone for optical insulation purposes
6. For better handling, e.g. mounting of the sensor to a micromanipulator, the microoptode was fixed with epoxy in a standard glass microcapillary (Fig. 1).

Fig. 1 is a schematic drawing of an oxygen microoptode. The insert shows the sensing layer covering the tapered tip. This method of indicator fixation proved to be stable enough for numerous profile measurements even in quartz sand without abrasion of significant amounts of indicator from the tip.

3. Measuring system

3.1. Phase-modulation technique

The luminescence lifetime was used as a measure of the oxygen-dependent quenching of luminescence to avoid the

problems that are inherent to intensity-based measurements. In the case of luminescence intensity measurements, it would be necessary to insulate the tapered fiber optically because otherwise the measured signal would strongly depend on the optical parameters of the environment. These parameters, like refractive index or absorption of the surrounding medium, are not constant while measuring in natural systems like marine sediments or biofilms. An optical insulation would increase the response time of the sensor by increasing the diffusion path length of oxygen molecules from the tip surroundings into the sensing layer. Furthermore, intensity fluctuations of the light sources or bleaching effects of the indicator have no impact on the lifetime measurement. So we have decided to use the luminescence lifetime of the described indicators as information and the well-known phase-modulation technique [5,7,13–16] to evaluate this lifetime.

If a luminophore is excited with sinusoidally intensity modulated light, its lifetime causes a time delay of the emitted light signal. In technical terms this delay is the phase angle between the exciting and emitted signal. This phase angle is shifted as a function of the oxygen concentration. The relation between lifetime τ and phase angle Φ is given by [14,16]

$$\tan(\Phi) = 2\pi f_{\mathrm{mod}}\tau \tag{3}$$

(f_{mod} = modulation frequency, Φ = phase angle, τ = luminescence lifetime).

Due to the non-linear nature of the tangent function, a proper choice of the modulation frequency is necessary. If the upper and lower lifetimes of analytical interest, τ_1 and τ_2, which are defined by the measuring range, are known, the optimum modulation frequency f_{opt} can be derived as

$$f_{\mathrm{opt}} = \frac{1}{2\pi\sqrt{\tau_1\tau_2}} \tag{4}$$

(f_{opt} = optimum modulation frequency, τ_1, τ_2 = luminescence lifetimes of analytical interest).

3.2. Optical setup

Fig. 2 shows the specially assembled optical setup of the microoptode array. It contains a combination of eight 2×2 fused-silica-glass couplers (E-Tek, San Jose, USA) that are assembled as follows: from the right to the left, one branch of each coupler is connected with standard ST-plugs to ST-receptacles with built-in optical filters and blue light-emitting diodes (Fig. 2, LED, λ_p = 450 nm, NSPB 500, Nichia Chemical Europe, Nürnberg, Germany). The second

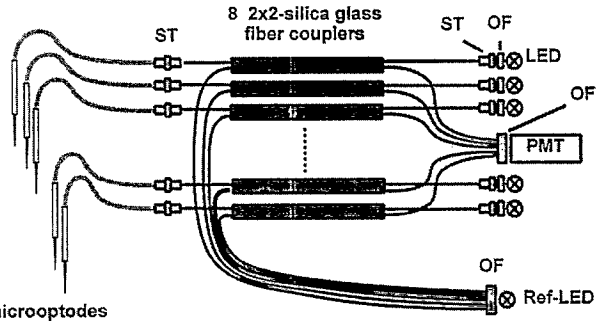

Fig. 2. The optical setup consists of eight 2×2 fused fiber couplers that have been specially assembled (see text for explanation): PMT, photomultiplier tube assembly; OF, optical filters; LED, light-emitting diode; Ref-LED, reference light-emitting diode; ST, standard fiber connectors and receptacles.

branches of the right side are combined to a fiber cable and coupled via a 600 μm silica-glass fiber and an optical long-pass filter (Fig. 2, OF) to a red-sensitive photomultiplier tube (Fig. 2, PMT, H5702-50, Hamamatsu, Herrsching, Germany). On the left side one branch of each coupler is connected to the microoptodes via standard ST-connectors, while the second branches are again combined to a cable and coupled via a 600 μm silica-glass fiber and an optical attenuation filter to a yellow LED (Fig. 2, Ref-LED, standard-type yellow LED) with a broad emission spectrum.

Each excitation LED can be addressed separately. In a time multiplex mode each of the excitation LEDs is switched on and off alternately with a frequency of 3 Hz to the red reference LED. This references the PMT and the whole electronic signal path except the excitation LED and its driving circuitry (this referencing idea is based on personal communications with Paul O'Leary and Christian Kolle, Joanneum Research, Graz, Austria and Ref. [7]).

3.3. Phase-angle detection

The phase-angle detection (Fig. 3) of the microoptode array uses a simple principle to convert the phase angle between two sinusoidal signals into a repetitive pulse width that can be converted into a d.c. signal by averaging.

The alternating optical signals of sensor and reference reach the PMT and the photocurrent is converted into a voltage and amplified (Fig. 3, PMT & I/U, v). Then the signal is bandpass filtered (extraction of the sinusoidal signal and reduction of noise) and amplified again (Fig. 3, BP, v). Now the signal is highpass filtered (reduction of amplifier offset influences) and is converted by a comparator or zero-crossing-detector (Fig. 3, Comp) into a rectangular signal.

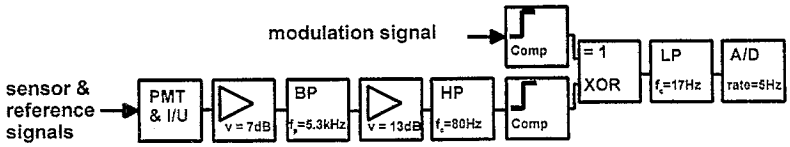

Fig. 3. Schematic drawing of the phase-angle detection: PMT & I/U, photomultiplier tube and current-to-voltage conversion; v, amplification; BP, electronic bandpass filter; f_p, peak frequency of bandpass filter; HP, electronic highpass filter; f_c, cutoff frequency; Comp, comparator; XOR, logical exclusive 'OR'; LP, electronic lowpass filter; A/D, analog-to-digital conversion; rate, sampling rate.

The modulation signal of the LEDs is also converted into a rectangular signal. Both signals are compared by a logical exclusive 'OR' (Fig. 3, XOR). The output of this operation is a rectangular signal at the same repetition frequency and a pulse width that is directly proportional to the phase-angle difference between incoming signal (measuring signal or reference signal) and modulation signal. This rectangular signal is lowpass filtered, which yields a linear relationship of Φ from 0° to 180°, corresponding to a d.c. voltage of 0 to 9.8 V, respectively. Finally the signal is converted into a digital signal (Fig. 3, LP, A/D) at a sampling rate of 6 Hz. The digital signal is further processed by a 16-bit microcontroller (NEC V25+, Däter+Müller, Berlin, Germany), which controls the microoptode array. As the signals are processed in a time multiplex regime, the indicator induced phase lag is the difference between the measured signal phase angle and reference phase angle. Additionally, the signal amplitude and d.c. value are processed in the analog processing unit and converted into digital values for control and possible further interpretations.

Table 2 gives an overview of the measuring system performance for both sensor types. The general phase-angle resolution according to the 12-bit A/D converters was 0.035°. The measured accuracy for sensor type A was $\Delta\Phi = \pm 0.07°$ and for sensor type B $\Delta\Phi = \pm 0.09°$. Expressed in oxygen values of percentage air saturation in water, this corresponds to an accuracy of approximately $\Delta O_2 = \pm 1\%$ air saturation for sensor A and $\Delta O_2 = \pm 0.3\%$ air saturation for sensor B. The non-equal accuracies for 0 and 100% air saturation reflect the non-linear Stern–Volmer relation. Although the accuracy in degrees is worse for the detection system of sensor B, the overall accuracy in oxygen values is better because of the larger signal change. The frequencies were chosen for a measuring range of 0–100% oxygen for possible applications in photosynthetically active sediments, where up to six times air saturation can be found. Therefore the presented range of phase angles in Table 2 does not seem to be symmetrical compared to the optimization criterion (Eq. (4)).

As can be seen in the schematic drawing of the first experimental setup (Fig. 4), the actual values were displayed simultaneously on an LCD display. The different running modes of the system were controlled via a front panel keypad as well as the amplification of the PMT via control of its high voltage. The data were sent via a serial interface (RS232) to a computer where data could be stored in ASCII format.

The sampling was performed one sensor after the other so the detection is only quasi-simultaneous. One scan took 43.2 s with 9.6 s per sensor, which was slightly slower than the sensor response time of ≈8 s. The displayed values in Fig. 3 are given for the system of sensor type B ($f_{mod} = 5.3$ kHz). For the measurements with sensor type A the system was adapted to the modulation frequency $f_{mod} = 44.7$ kHz.

4. Experimental applications of the microoptode array

(A) For first investigations of the temperature behavior of the oxygen microoptodes (type A), the sensors were positioned in a special calibration vessel (Fig. 4). This vessel consisted of two vessels: (a) a water-filled inner vessel that was perfused with preheated defined gas mixtures, derived from nitrogen and air; (b) an outer vessel that was constantly perfused with thermostatted water to control the temperature of the inner vessel and keep it constant. With this setup six calibration points at different gas mixtures were measured to determine the calibration parameters of the micro optodes. The procedure was repeated at different temperatures. Additionally, the uniformity of each channel of the array was tested with one microoptode sequentially connected to all channels at a defined gas mixture and temperature.

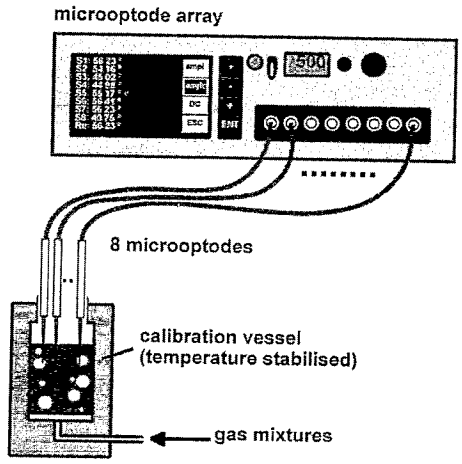

Fig. 4. Thermostatted experimental setup for temperature and calibration measurements: eight oxygen microoptodes, sensor type A, were positioned in a calibration vessel that consisted of an inner vessel filled with water and an outer vessel that was perfused with thermostatted water. The inner vessel was perfused with defined gas mixtures. The instrument displays the measured data of each sensor simultaneously and can send the data via a serial interface (RS232) to a PC for data storage (not shown).

(B) A long-term experiment was performed in a diffusion chamber setup. In Fig. 5 it can be seen that both chambers were separated by an initially 11 mm thick agar layer. Four

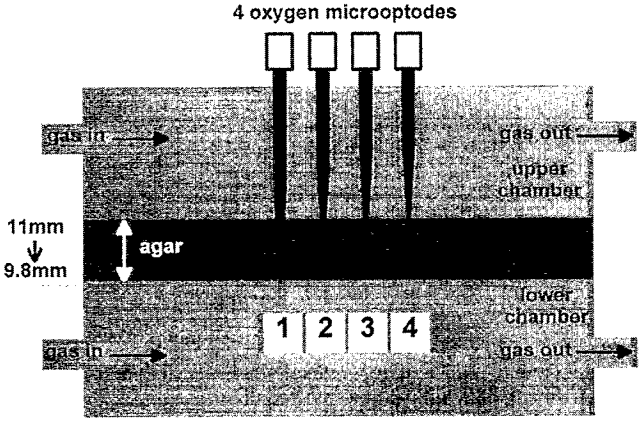

Fig. 5. Experimental setup for long-term measurement with four oxygen microoptodes (type A): the two gas chambers were separated by an ≈11 mm thick agar layer. The perfusing gases, nitrogen and room air, were humidified to prevent the agar from shrinking. The microoptodes were positioned at different depths from the upper agar surface: [1] 10.2 mm, [2] 7.5 mm, [3] 4.5 mm and [4] 2.1 mm.

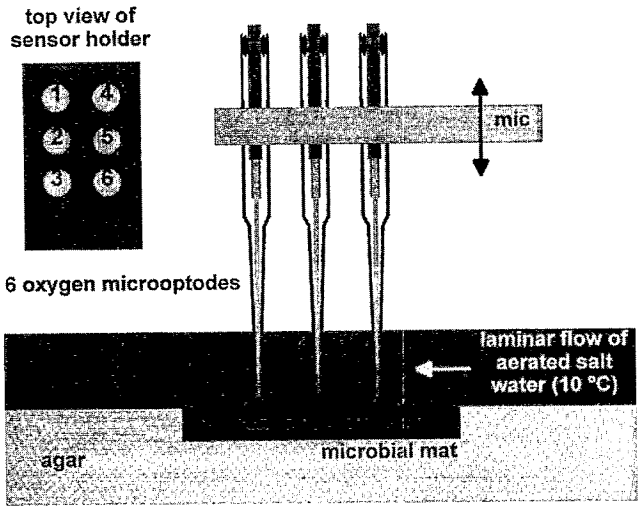

Fig. 6. Experimental setup for oxygen depth profiles: the microbial mat was fixed in an agar layer and flushed with a nearly laminar flow of aerated salt water at a temperature of 10°C. Six oxygen microoptodes (type B) were mounted in a sensor holder that is fixed in a micromanipulator (mic). The profiles were measured in steps of 100 μm. The position numbers in the top view refer to the measured oxygen profiles in Fig. 9.

microoptodes of type A were positioned at different depths to observe the oxygen diffusion in defined distances to the surface. The whole setup was in a climate room at a constant temperature of 15°C. The gases, nitrogen and air, were moistened to prevent the agar from shrinking. Nevertheless, the agar shrunk over the period of a few days from 11 to 9.8 mm thickness; this is illustrated in Fig. 5 with the microoptode at position 1 which punches through the agar layer.

(C) The microoptode array was applied to a natural system to measure oxygen depth profiles. The investigated object was a piece of a microbial mat with a dense population of cyanobacteria from Solar Lake, Egypt. The mat was placed in an agar layer in a flow chamber (Fig. 6). Above the mat was a constant nearly laminar flow of aerated salt water at 10°C. The whole setup was in a climate room at the same temperature. Six oxygen microoptodes of type B in a special sensor holder (Fig. 6) were fixed to a micromanipulator (Fig. 6, mic) and each sensor was positioned in the sensor holder in such a way that, ±20 μm, each sensor touched the water surface. The profile measurements were performed in steps of 100 μm. During the measurement one sensor broke, so the results show only five profiles.

5. Results

(A) Sensor type A is only slightly temperature dependent. The left graph in Fig. 7 shows the quenching efficiency K_{SV} as a function of the temperature for eight oxygen microoptodes of type A and the right graph gives the corresponding lifetime values τ_0 at zero oxygen. The values are normalized to the value at 3.7°C. The quenching efficiency shows an increase of 32% over a temperature difference of 35°C, while the lifetime at zero oxygen only shows a decrease of 16% for the same range (Fig. 7, right graph). However, it demonstrates the necessity to measure the calibration values at the same temperature as the measurement or to measure the temperature as well to be able to correct the measuring signals. The results of the uniformity measurements showed differences of maximum 1° offset in phase angle between each channel. These variations are due to differences between the LEDs and their driving circuits, which are not referenced by the present method. The LEDs reach a thermal steady state faster than the PMT, so it is possible to treat the differences as constant offset phase angles and correct for them mathematically by subtraction or addition to the measured phase angle of each channel. The use of the array eases the characterization procedure for microoptodes because eight microoptodes can be measured simultaneously.

(B) Fig. 8 shows the whole time course of a diffusion experiment that finally led to a reconstruction of the experimental setup. At the beginning both chambers (Fig. 5, upper and lower chamber) were perfused with nitrogen to get the system oxygen free. After 12 h at point t_1 (Fig. 8) the nitrogen tank became empty. This was noticed 20 min later; a full nitrogen tank was connected but we did not wait long enough

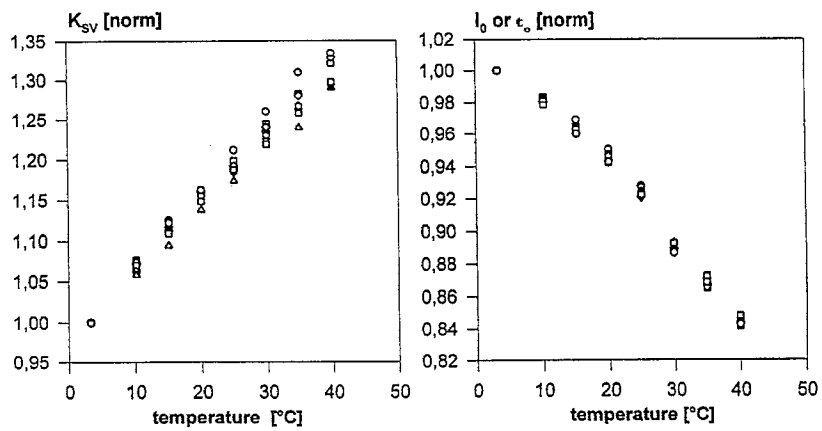

Fig. 7. Calibration and temperature measurements with eight oxygen microoptodes (type A) at different temperatures: the quenching coefficient and the lifetime or intensity in absence of oxygen are shown at different temperatures. Both are normalized to the measured values at a temperature of 3.7°C.

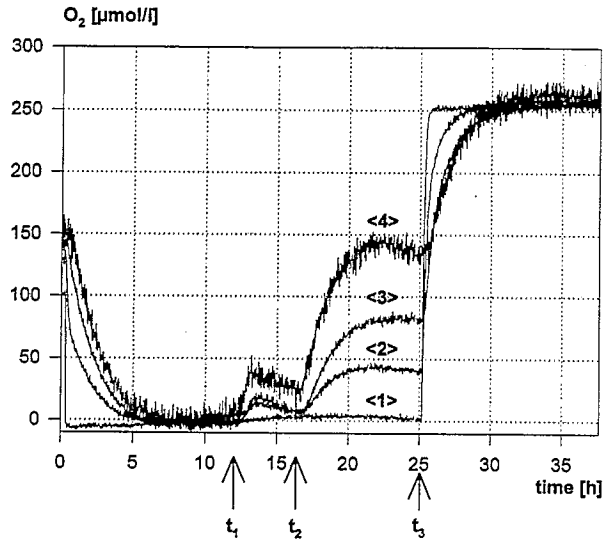

Fig. 8. Longterm measurement: the measured oxygen vs. time of the experiments is shown over a period of 37 h. The numbers of the curves correspond to the sensor depths in Fig. 5, while the special events t_1, t_2 and t_3 are explained in the text.

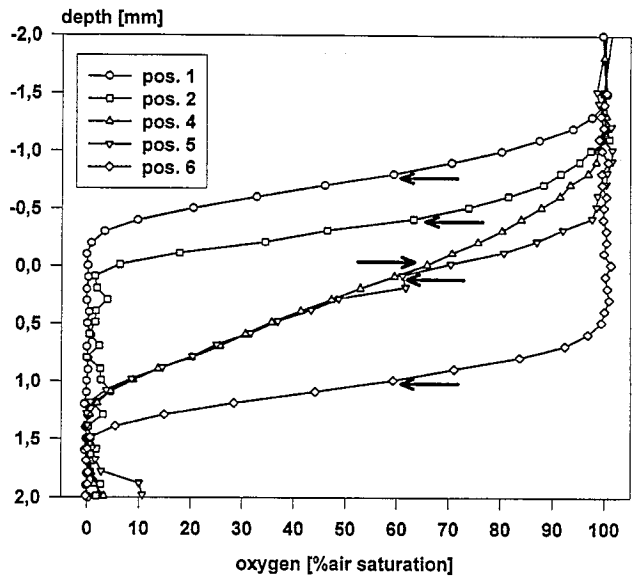

Fig. 9. Oxygen depth profiles with five oxygen microoptodes, sensor type B: penetration depth vs. measured oxygen (negative direction means above surface). The profiles are corrected in a way that all sensors would touch the surface simultaneously. The arrows indicate the sediment surface position for each sensor.

to reach an oxygen-free steady state. After 17 h at point t_2 (Fig. 8) the gas connection of the upper chamber was switched to room air and diffusion of air into the agar took place from above. At point t_3, 25 h after having started the experiment, the gas connection of the lower chamber was also switched to room air. While the sensors at positions 2–4 (Fig. 8) nicely follow the oxygen diffusion at their respective depths, the punched-through sensor at position 1 (Fig. 8) directly follows the gas mixture in the lower chamber. The higher noise of the sensor at position 4 (Fig. 8) is related to a smaller overall signal size of the sensor and reflects a worse signal-to-noise ratio compared to the other sensors. The microoptode array proved to give stable recordings for long-term experiments.

(C) Oxygen depth profiles (Fig. 9) were measured in a respiring microbial mat. The profiles are normalized in a way that all the sensors would touch the water surface parallel to the sensor at position 1. This was necessary because some of the sensors were not fixed well enough and were a little displaced ($\approx$20–30 µm) after repeated measurements. This was measured after the experiment and has been corrected in Fig. 9. So the different depth positions of each profile reflect the differences in the surface structure of the mat. The surface penetration of each sensor is indicated by the arrows in Fig. 9. The differences in the slopes of the oxygen depth profiles illustrate the heterogeneity of the oxygen distribution found in most natural systems and demonstrate the necessity to measure a profile distribution instead of a single profile when quantitative studies of oxygen consumption should be done.

The deviations of the profiles of the sensors at positions 4 (Fig. 9, depth = 0.2 mm) and 5 (Fig. 9, the rise of oxygen in the curve of position 5 below 1.5 mm) are due to an additional problem that may occur if optical sensors are applied to natural systems. The light also leaves the fiber tip so, depending on the composition of the microbial mat, it can excite natural chlorophyll fluorescence that interferes with the signal. As this amount of noise signal is not constant, it cannot be corrected for. We are currently trying to reduce the amount of light leaving the fiber, to optimize the optical filter sets to minimize the effect or to switch to other indicators with more suitable excitation wavelength ranges. Multifrequency approaches for separating the noise signal from the information are also being investigated.

6. Conclusions

The presented experiments demonstrate some of the possible applications of the new microoptode array. Although there are some variations or offsets between each channel due to electronic properties of the LED driving circuits or the LEDs themselves, they can be corrected for. Another problem of the present optical setup is that even though the sensor excitation can be selected, the background signal from ambient light is summed up. So the array has an eight times higher background signal compared to a single-channel measuring device [5]. This makes applications with large amounts of ambient light problematic because of the conflict between high sensitivity of the PMT and its dynamics. According to this restriction we are currently developing a new array with a 1×8 optical switch for a comparative study that should define the best applications for each array. However, in many applications with dark incubated sediments or moderately illuminated setups, the presented microoptode array has demonstrated its good performance. It is possible to get a maximum of eight oxygen depth profiles with one profiling

procedure, to measure and observe the oxygen concentration in different depths at the same time, and to observe the oxygen value at different points in the same setup or in different setups.

Acknowledgements

We gratefully acknowledge G. Hertz for his support in mechanical construction and fabrication of the microoptode array. We thank the Commission of the European Community for support under the MAST III Programme MICROMARE, project no. 950029.

References

[1] B.B. Jørgensen and N.P. Revsbech, Colorless sulfur bacteria, Beggiatoa spp. and Thiovolum spp. in O_2 and H_2S microgradients, *Appl. Environ. Microbiol., 45* (1983) 1261–1270.

[2] N.P. Revsbech and B.B. Jørgensen, Microelectrodes: their use in microbial ecology, in K.C. Marshall (ed.), *Advances in Microbial Ecology*, Vol. 9, Plenum, New York, 1986, pp. 293–352.

[3] I. Klimant, V. Meyer and M. Kühl, Fiber-optic oxygen microsensors, a new tool in aquatic biology, *Limnology Oceanography, 40* (1995) 1159–1165.

[4] I. Klimant, G. Holst and M. Kühl, Oxygen microoptrodes and their application in aquatic environment, *SPIE Proc.*, Vol. 2508-45, *Chemical, Biochemical and Environmental Fibre Sensors VII, Munich, Germany, 19–23 June, 1995*, pp. 375–386.

[5] G. Holst, M. Kühl and I. Klimant, A novel measuring system for oxygen micro optodes based on a phase modulation technique, *SPIE Proc.*, Vol. 2508-45, *Chemical, Biochemical and Environmental Fibre Sensors VII, Munich, Germany, 19–23 June, 1995*, pp. 387–398.

[6] O. Stern and M. Volmer, Über die Abklingzeit der Fluoreszenz, *Phys. Z., 20* (1919) 183–188.

[7] J.R. Alcala, C. Yu and G.J. Yeh, Digital phosphorimeter with frequency domain signal processing: application to real-time fiber-optic oxygen sensing, *Rev. Sci. Instrum., 64* (1993) 1554–1560.

[8] H. Kautsky, Quenching of luminescence by oxygen, *Trans. Faraday Soc., 35* (1939) 216–219.

[9] D.W. Lübbers and N. Opitz, The pCO_2/pO_2 optrode: A new probe for measuring pCO_2 and pO_2 of gases and liquids, *Z. Naturforsch., 30C* (1975) 532–533.

[10] I. Bergman, Rapid response atmospheric oxygen monitor based on fluorescence quenching, *Nature, 218* (1986) 396.

[11] J.M. Vanderkooi and D.F. Wilson, A new method of measuring oxygen concentration in biological systems, *Adv. Exp. Med., 200* (1986) 189–193.

[12] J.R. Bacon and J.N. Demas, Determination of oxygen concentrations by luminescence quenching of a polymer immobilized transition-metal complex, *Anal. Chem., 59* (1987) 2780–2785.

[13] M.E. Lippitsch, J. Pusterhofer, M.J.P. Leiner and O.S. Wolfbeis, Fibre-optic sensor with the fluorescence decay time as the information carrier, *Anal. Chim., 205* (1988) 1–6.

[14] J.R. Lakowicz, *Principles of Fluorescence Spectroscopy*, Plenum, New York, 3rd. edn., 1983.

[15] O.S. Wolfbeis, *Fiber Optic Chemical Sensors and Biosensors*, Vols. I+II, CRC Press, Boca Raton, 1991.

[16] K.W. Berndt and J.R. Lakowicz, Electroluminescent lamp-based phase fluorometer and oxygen sensor, *Anal. Biochem., 201* (1992) 319–325.

[17] P. Hartmann, M.J.P. Leiner and M.E. Lippitsch, Luminescence quenching behavior of an oxygen sensor based on a Ru(II) complex dissolved in polystyrene, *Anal. Chem., 67* (1995) 88–93.

[18] D.B. Papkovsky, New oxygen sensors and their application to biosensing, *Sensors and Actuators B, 29* (1995) 213–218.

Biographies

Gerhard Holst, born in 1962, studied electronic engineering at the RWTH University in Aachen, Germany, where he received the diploma in 1990 with a final work about reflectance pulse oximetry with electrooptical and hybrid fiber-optical sensors. From 1991 to 1994 he completed his Ph.D. in the group of Professor D.W. Lübbers at the Max-Planck-Institute for Molecular Physiology, Dortmund, Germany, about a new optical chemical-sensing principle, the oxygen flux optode, and its phase-modulation-based measuring system. In 1994 he joined the Microsensor Research Group of the Max-Planck-Institute for Marine Microbiology, Bremen, Germany as a postdoctoral fellow, where he is currently working on the development of new fiber-optic microsensors, microoptodes, and their time-resolved measuring schemes and systems for laboratory and field applications.

Ronnie N. Glud, born in 1963, studied biology at the University of Aarhus, Denmark, where he received an M.Sc. degree in microbial ecology 1990 with a thesis on the application of microsensors in photosynthetic biofilms. From 1990 to 1993 he completed his Ph.D. at the Department of Microbial Ecology, University of Aarhus, Denmark. His Ph.D. work focused on in situ studies of oxygen dynamics and early diagenetic processes in marine sediments. In 1993 he joined the Max-Planck-Institute for Marine Microbiology, Bremen, Germany, as a postdoctoral fellow. His scientific interests are in situ studies of benthic mineralization with special emphasis on oxygen dynamics.

Michael Kühl, born in 1964, studied biology at the University of Aarhus, Denmark, where he received an M.Sc. degree in microbial ecology in 1988 with a thesis on the development of fiber-optic microprobes and a measuring system for microscale light measurements in sediments and biofilms. From 1988 to 1992 he completed his Ph.D. at the Department of Microbial Ecology, University of Aarhus, Denmark. His Ph.D. work involved the use of both optical and electrochemical microsensors to study the microenvironment in compact microbial communities. In 1992 he joined the Max-Planck-Institute (MPI) for Marine Microbiology, Bremen, Germany, as a postdoctoral fellow to build up microsensor research at the institute. Since 1995 he has been the head of the Microsensor Research Group at the MPI in Bremen. His scientific interests are the development and use of fiber-optic and electrochemical microsensors in microbial ecology.

Ingo Klimant, born in 1964, graduated in analytical chemistry at the Bergakademie Freiberg, Germany, in 1990. In

1993 he received a Ph.D. in chemistry from the Karl-Franzens University in Graz, Austria. His work involved the design of optical sensing schemes for oxygen and ammonia. From 1994 to 1996 he worked as a postdoctoral fellow at the Max-Planck-Institute for marine Microbiology in the Microsensor Research Group and developed a variety of microoptodes for application in aquatic environments. Since 1996 he has been at the Institute for Analytical Chemistry, Bio- and Chemical Sensors at the University of Regensburg, Germany. His scientific interest is the development of optical and optical chemical microsensors and their sensing schemes for application in biological systems.